Introduction

In this work we propose to present the application istropic Elastic Full Waveform Inversion (E-FWI) to a real dataset. The studied area is located within the Loranca Basin (Spain), and present a smooth topography which is part of the challenge propose here. In order to characterize the very shallow surface, a 3D seismic data volume jointly with various 2D electrical line surveys were acquired in a square area of 540x540 m^2. Although originally designed to perform a high resolution travel-time tomography, it would be of great interest to tak advantage of the data to perform FWI. We propose to perform E-FWI because the target structures are close to the surface (< 120 m deep) making wave propagation to be mostly driven by elastic effects. On the other hand, it has proven to be more resolutive than its acoustic version, providing clear imaging improvements (Vigh et al., 2014; Raknes et al., 2015).

This dataset is part of ongoing multidisciplinary geophysical, geological, hydrological characterization of an area which has been proposed as a possible site to host a temporal radioactive waste disposal site. Therefore, a large amount of multidisciplinary data revealing information on the underground is available including down-hole measurements and other geophysics.

In our scenario, we include free-surface effects, and consequently take topography into account. We will show that the resulting models provides a better understanding of the geological features and that there are also show a good correlation with borehole measurements.

Theory

On one hand, we use the time-domain elastic isotropic approach for solving the elastic wave equation by means Full staggered grid combined with mimetic operators (de la Puente et al., 2014)

$$\begin{aligned} \rho(\mathbf{x})\dot{\mathbf{v}}(\mathbf{x},t) &= \nabla\cdot\boldsymbol{\sigma}(\mathbf{x},t)+\mathbf{f}_s(\mathbf{x}_s,t), \\ \dot{\boldsymbol{\sigma}}(\mathbf{x},t) &= \mathbf{C}(\mathbf{x}):\ \nabla\mathbf{v}(\mathbf{x},t) \end{aligned} \tag{1}$$

where f_s is the source function at position $\mathbf{x}_s$, $\mathbf{v}$ the particle velocity, ρ the density (set as a constant), and $\boldsymbol{\sigma}$ the stress field, and therefore take topography into account.

On the other hand, the mathematical formulation of FWI consists of the minimization of a function error $E(\mathbf{m},\mathbf{m}_{real})$ (Pratt, 1999; Virieux and Operto, 2009), where $\mathbf{m}$ and $\mathbf{m}_{\text{real}}$ are the current and target model respectively. In this study we employ the normalized least-square criterion L^2 given by

$$E_k(\mathbf{m}_{\text{k}},\mathbf{m}_{\text{ real}}) = \frac{1}{2}\sum_{i=1}^{N}\sum_{j=1}^{n}\left[\frac{\mathbf{u}_j^i(\mathbf{x}_{\text{r}},\mathbf{x}_{\text{s}};\mathbf{m}_k)}{\max_j(|\mathbf{u}^i(\mathbf{x}_{\text{r}},\mathbf{x}_{\text{s}};\mathbf{m}_k\ )|)}-\frac{\mathbf{u}_j^i(\mathbf{x}_{\text{r}},\mathbf{x}_{\text{s}};\mathbf{m}_{\text{real}})}{\max_j(|\mathbf{u}^i(\mathbf{x}_{\text{r}},\mathbf{x}_{\text{s}};\mathbf{m}_{\text{real}})|)}\right]^2, \tag{2}$$

where N is the number of receivers, n the number of samples of each trace, $\mathbf{x}_{\text{r}}$ and $\mathbf{x}_{\text{s}}$ are the receiver and source position respectively, $\mathbf{u}(\mathbf{x}_{\text{r}},\mathbf{x}_{\text{s}};\mathbf{m}_k)$ and $\mathbf{u}(\mathbf{x}_{\text{r}},\mathbf{x}_{\text{s}};\mathbf{m}_{\text{real}})$ stand for the displacement from the current model parameters at the k^{th} iteration and for the experimental dataset respectively.

Our approach for E-FWI consists in constraining the maximum offset to the longest wavelength at the present frequency. We call this approach Dynamic Offset Control (DOC). It aims to use smaller offset for reflection data when increasing frequency. Thus, we select the offset according to

$$Offset = V/f_0 \tag{3}$$

where f_0 is the cut-off frequency of the low-pass filter applied to the data and V a parameter to be defined by user. This strategy has the side effects of reducing the computational domain as we go into higher

frequencies while minimizing the effect of the surface waves on the gradients. We numerically found that V equal to $\max(V_p)$ shows to be a sufficient condition. We want to stress that the computational grid is adapted to the shortest wavelength present in the models and does not match the receivers and sources grids. Besides, no part of the model has been fixed.

We apply gradient preconditioning in two steps: first we look for the $log(m)$ instead of m, and secondly we use the square of the illumination. In all our tests, it shows to be an efficient preconditioner.

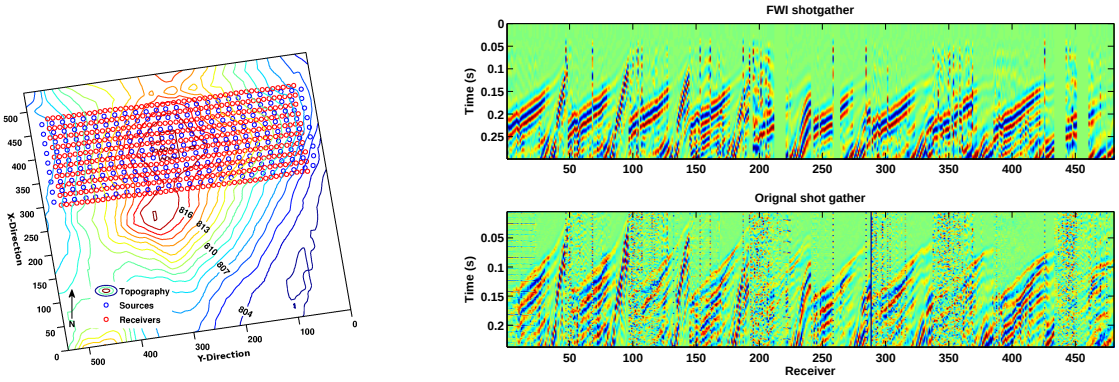

(a) (b)

Figure 1: (a) Aquistion geometry: Topgraphy is smooth; sources and receivers are the blue and red circles respectively. (b) Shotgather normalized trace by trace: after acquisition (bottom) and after pre-processing and bad traces removal (top).

3D Elastic Full Waveform Inversion

The acquisition setup is shown in Fig. 1(a): it consists in 9 shooting lines and 10 recording lines of 48 geophones each. The total acquisition time is 2 s. Nevertheless, we picked the first arrivals, and apply a window of 0.2 s around them, in order to take advantage of both surface and compressional waves. The density is set to be constant as we are focusing on phase rather than to the amplitude. Q effects are strongly attenuated by the misfit function and are neglected too. The starting model for V_p is obtained from Travel-Time Tomography (TTT) (Tryggvason et al., 2002), and half of V_p for V_s. We denoised the data with a band-pass filter (ranging from 10-40 Hz) applied two times, and deleted the worst traces following a mean criterion. After pre-processing, we keep around a 80% of the total amount of the data available (see Fig. 1(b)). The inversion strategy is summarized in Table 1, and consists in low-pass filtering, and data selection according the DOC criterion. The total computational time was 72 hours runnning on 75 nodes of Mare Nostrum supercomputer.

Frequency	15 Hz	20 Hz	25 Hz
Mesh size	40x169x169	48x201x201	56x237x237
DOC	306	230	180
Iteration	15	15	15

Table 1: Multi-grid and multi-scale parameters for 2D FWI. From top to bottom: cut-off frequency, mesh size, spatial discretization, and number of iterations.

Figure 2 presents depth slices of the velocity fields at depth 25, 50, 75, and 100 m obtained after inversion. We observe in general that the compressional velocities have been overestimated by TTT, which

also could be observed on the synthetic traces obtained at the first iteration of the first frequency: predicted time arrivals are earlier to those recorded (see Fig. 3(a)). Consequently, FWI lowered velocities as observed in Fig. 2.

In Fig. 3, we present the comparison of 4 traces equally spaced along receivers line 8 of shot 813 (Line 8, shot 13) for the final inverted models (in blue) and the seismograms predicted by the starting model (in dash green) at frequency 25 Hz. We observe that the velocity models allow to predict much better the travel times of the recorded data. Finally, fittings of the borehole SVC6 with velocity depth profiles (located near the borehole but not at the exact position) have also been improved respect to those from the starting models: we observed good agreement of the low-frequency content for both V_s and V_p (see Fig. 3).

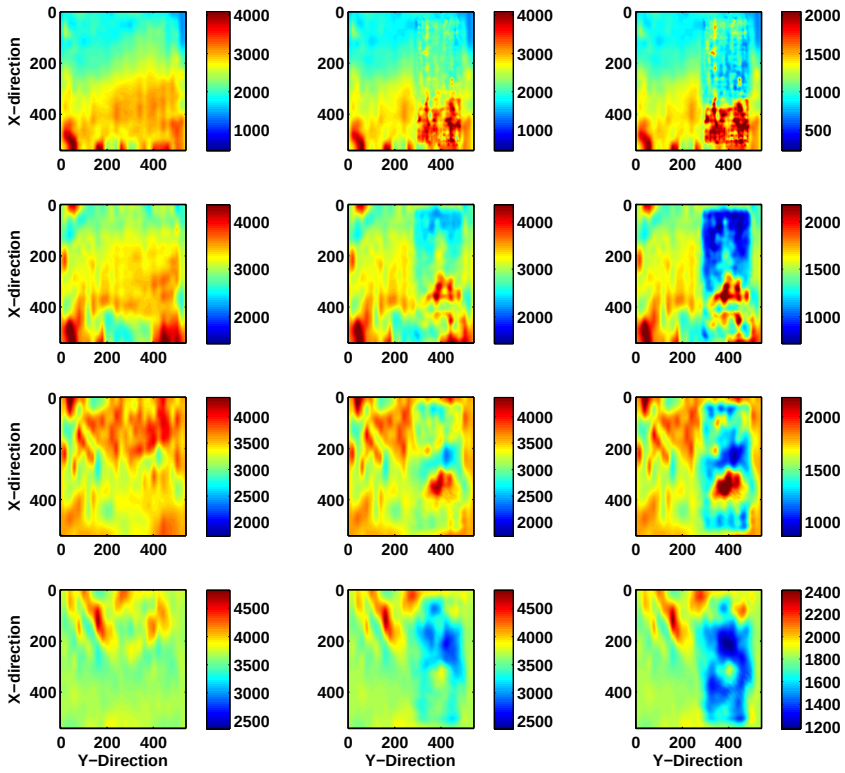

Figure 2: Four detph slice for V_p and V_s velocities. From left to right: V_p starting model, inverted V_p, and inverted V_s. From top to bottom: depth 25, 50, 75, and 100 m.

Conclusions

We have presented a 3D Elastic FWI successfully working on real data in presence of topography, using only near-source offsets. purpose, we have introduced an offset selection method called Dynamic Offset Control. This technique allows to reduce the maximum aperture of each shot in FWI, hence reducing the computational cost when moving into higher frequencies, a key point for elastic inverison. E-FWI clearly improves the knowledge of the shallow subsurface structures, as observed when comparing inverted models with the borehole measurements.

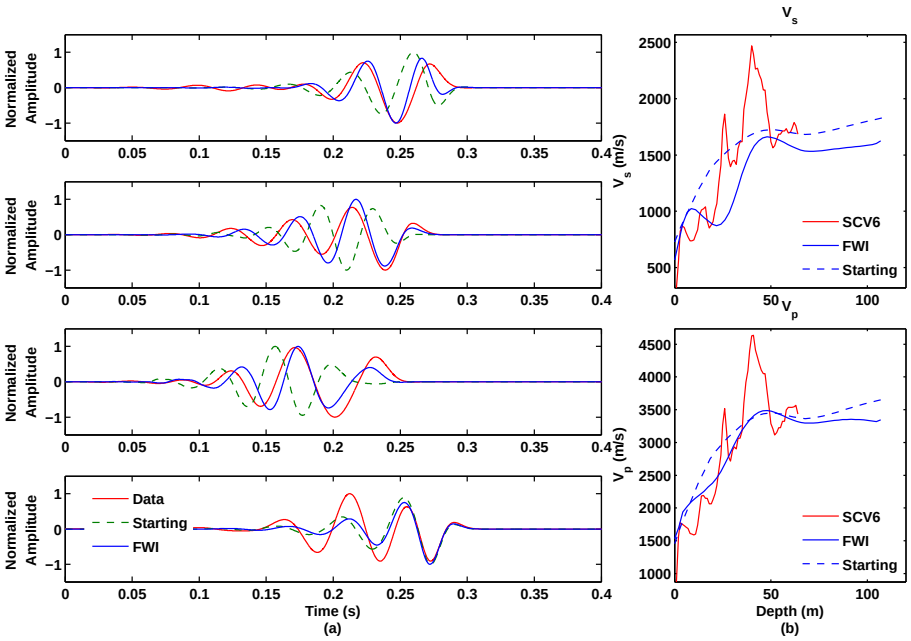

Figure 3: V_p and V_s (top to bottom) profiles obtained with the strategy of Table 1 at range 6, 9 and 12 Km (left to right). The inverted, starting and target models (blue, dash and red line respectively).

Acknowledgements

The authors thank Repsol for the permission to publish the present research and for funding through the Aurora project. J. Kormann also thankfully acknowledges the Spanish Supercomputing Network (RES) through grant FI-2014-2-0009. Funding support for the data acquisition and access to the available geophysical data was provided by ENRESA. The GFZ Instrument Pool provided the instrumentation for the data acquisition. This project was partially funded by the European Union's Horizon 2020 research and innovation programme under the Marie Sklodowska-Curie grant agreement No 644602.

References

Pratt, R.G. [1999] Seismic waveform inversion in the frequency domain, Part 1: Theory and verification in a physical scale model. *Geophysics*, **64**, 888–901.

de la Puente, J., Ferrer, M., Hanzich, M., Castillo, J.E. and Cela, J.M. [2014] Mimetic seismic wave modeling including topography on deformed staggered grids. *Geophysics*, **79**(3), T125–T141.

Raknes, E.B., Arntsen, B. and Weibull, W. [2015] Three-dimensional elastic full waveform inversion using seismic data from the Sleipner area. *Geophysical Journal International*, **202**, 1877âĂŞ1894.

Tryggvason, A., Rögnvaldsson, S. and Flovenz, Ó.G.. [2002] Three-dimensional imaging of P- and S-wave velocity structure and earthquake locations beneath southwest Iceland. *Geophysical Journal International*, **171**(5), 848–866.

Vigh, D., Jiao, K., Watts, D. and Sun, D. [2014] Elastic full-waveform inversion application using multicomponent measurements of seismic data collection. *Geophysics*, **79**(2), R63–R77.

Virieux, J. and Operto, S. [2009] An overview of full-waveform inversion in explorat ion geophysics. *Geophysics*, **74**, WCC127–WCC152.